Article

Assembly of Well-Aligned Multiwalled Carbon Nanotubes in Confined Polyacrylonitrile Environments: Electrospun Composite Nanofiber Sheets

Jason J. Ge, Haoqing Hou, Qing Li, Matthew J. Graham, Andreas Greiner, Darrell H. Reneker, Frank W. Harris, and Stephen Z. D. Cheng

J. Am. Chem. Soc., **2004**, 126 (48), 15754-15761• DOI: 10.1021/ja048648p • Publication Date (Web): 10 November 2004

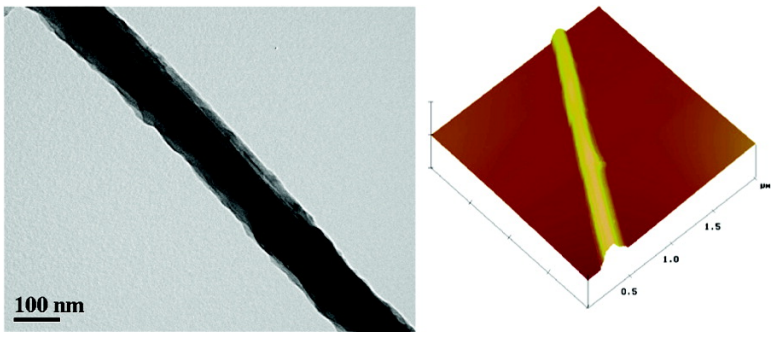

More About This Article

Additional resources and features associated with this article are available within the HTML version:

- Supporting Information
- Links to the 11 articles that cite this article, as of the time of this article download
- Access to high resolution figures
- Links to articles and content related to this article
- Copyright permission to reproduce figures and/or text from this article

View the Full Text HTML

J|A|C|S
ARTICLES
Published on Web 11/10/2004

Assembly of Well-Aligned Multiwalled Carbon Nanotubes in Confined Polyacrylonitrile Environments: Electrospun Composite Nanofiber Sheets

Jason J. Ge,[||] Haoqing Hou,[‡] Qing Li,[†] Matthew J. Graham,[†] Andreas Greiner,[§] Darrell H. Reneker,*[,†] Frank W. Harris,[†] and Stephen Z. D. Cheng*[,†]

Contribution from the Maurice Morton Institute and Department of Polymer Science, The University of Akron, Akron, Ohio 44325; Chemistry College of Jiangxi Normal University, Nanchang, JX 330027, China; Materials Science Center, Department of Chemistry, Philipps-University Marburg, Hans-Meerwein-Strasse, 35032 Marburg, Germany

Received March 9, 2004; Revised Manuscript Received July 20, 2004; E-mail: dhr@polymer.uakron.edu; scheng@uakron.edu

Abstract: Highly oriented, large area continuous composite nanofiber sheets made from surface-oxidized multiwalled carbon nanotubes (MWNTs) and polyacrylonitrile (PAN) were successfully developed using electrospinning. The preferred orientation of surface-oxidized MWNTs along the fiber axis was determined with transmission electron microscopy and electron diffraction. The surface morphology and height profile of the composite nanofibers were also investigated using an atomic force microscope in tapping mode. For the first time, it was observed that the orientation of the carbon nanotubes within the nanofibers was much higher than that of the PAN polymer crystal matrix as detected by two-dimensional wide-angle X-ray diffraction experiments. This suggests that not only surface tension and jet elongation but also the slow relaxation of the carbon nanotubes in the nanofibers are determining factors in the orientation of carbon nanotubes. The extensive fine absorption structure detected via UV/vis spectroscopy indicated that charge-transfer complexes formed between the surface-oxidized nanotubes and negatively charged (—C≡N:) functional groups in PAN during electrospinning, leading to a strong interfacial bonding between the nanotubes and surrounding polymer chains. As a result of the highly anisotropic orientation and the formation of complexes, the composite nanofiber sheets possessed enhanced electrical conductivity, mechanical properties, thermal deformation temperature, thermal stability, and dimensional stability. The electrical conductivity of the PAN/MWNT composite nanofibers containing 20 wt % nanotubes was enhanced to ~1 S/cm. The tensile modulus values of the compressed composite nanofiber sheets were improved significantly to 10.9 and 14.5 GPa along the fiber winding direction at the MWNT loading of 10 and 20 wt %, respectively. The thermal deformation temperature increased with increased MWNT loading. The thermal expansion coefficient of the composite nanofiber sheets was also reduced by more than an order of magnitude to 13 $\times$ 10^{-6}/°C along the axis of aligned nanofibers containing 20 wt % MWNTs.

Introduction

Both single-walled carbon nanotubes (SWNTs) and multi-walled carbon nanotubes (MWNTs) are of scientific interest in nanotechnology and nanodevices because of their superior structural, mechanical, chemical, thermal, and electrical performance.[1−4] In SWNT studies, the highest modulus for polymer/SWNTs microfibers with a diameter above several micrometers (up to ~50 GPa) was developed with the aid of sodium dodecyl sulfate (SDS) and poly(vinyl alcohol) (PVA) as interfacial binding agents in a coagulation based process.[5,6] In addition, SWNT reinforced pitch-based carbon microfibers[7] and polyacrylonitrile (PAN)/SWNT microfibers[8] exhibited a significant improvement in mechanical properties, thermal stability, and glass transition temperatures (T_g). A similar observation was reported for poly(*p*-phenylene benzobisoxazole) (PBO)/SWNT microfibers.[9] The PAN polymers are of particular interest, since they are used commercially as carbon fiber precursors. MWNTs are easier to produce at low cost than single-walled carbon nanotubes, but their concentric nano-

[†] The University of Akron.
[‡] Chemistry College of Jiangxi Normal University.
[§] Philipps-University Marburg.
[||] Current address: jge@nanofilm.cc, Nanofilm, 10111 Sweet Valley Drive, Valley View, OH 44125.

(1) Iijima, S. *Nature* **1991**, *354*, 56.
(2) Baughman, R. H.; Zakhidov, A. A.; de Heer, W. A. *Science* **2002**, *297*, 787.
(3) Collins, P. G.; Arnold, M. S.; Avouris, Ph. *Science* **2001**, *292*, 706.
(4) Yu, M.-F.; Lourie, O.; Dyer, M. J.; Moloni, K.; Kelly, T. F.; Ruoff, R. S. *Science* **2000**, *287*, 637.
(5) Vigolo, B.; Penicaud, A.; Coulon, C.; Sauder, C.; Pailler, R.; Journet, C.; Bernier, P.; Poulin, P. *Science* **2000**, *290*, 1331.
(6) Baughman, R. H. *Science* **2000**, *290*, 1310.
(7) Andrews, R.; Jacques, D.; Rao, A. M.; Rantell, T.; Derbyshire F.; Chen, Y.; Chen, J.; Haddon, R. C. *Appl. Phys. Lett.* **1999**, *75*, 1329.
(8) Sreekumar, T. V.; Liu, T.; Min, B. G.; Guo, H.; Kumar S.; Hauge, R. H.; Smalley, R. E. *Adv. Mater.* **2004**, *16*, 58.
(9) Kumar, S.; Dang, T. D.; Arnold, F. E.; Bhattacharyya, A. R.; Min, B. G.; Zhang, X.; Vaia, R. A.; Park, C.; Adams, W. W.; Hauge, R. H.; Smalley, R. E.; Ramesh S.; Willis, P. A. *Macromolecules* **2002**, *35*, 9039.

10.1021/ja048648p CCC: $27.50

structures are complicated by roll-up vector directions (chirality), crystallographic defects, and imperfect structures.

To effectively transfer the superior properties of the carbon nanotubes to nanocomposites, critical challenges lie in achieving strong interfacial bonding between the nanotubes and polymers while maintaining flexibility and good processibility. For well dispersed carbon nanotubes in organic or polymer systems, both covalent functionalization of the carbon nanotubes[10−13] and noncovalent attachment by physical $\pi-\pi$ stacking interactions[14−16] are needed to form strong interfacial bonding between nanotubes and the polymer matrix. Achieving a high concentration of the nanotubes in the polymer remains as a major barrier to overcome.

Electrospinning is a nanofiber assembly technique that utilizes an external electrostatic field to generate high surface areas on small fibers with diameters on the nanometer scale.[17,18] The polymer solution is contained in a reservoir with a charged capillary tip. Incorporation of carbon nanotubes into nanofibers has been demonstrated to enhance electrical conductivity in conductive polyurethane/polyaniline/MWNT and poly(vinylidene fluoride)/SWNT composite nanofibers.[19,20] Improved thermal stability and Young's modulus in PAN/SWNT nanofibers were also observed.[21,22] In these reports, the orientation and distribution of the nanotubes in the nanofibers were macroscopically random. Recently, locally oriented nanotubes embedded in nanofibers electrospun from poly(ethylene oxide)-(PEO)/SDS/MWNT and PEO/Gum Arabic/MWNT were observed using transmission electron microscopy, in which SDS and Gum Arabic were used as binding agents in aqueous dispersions.[23] However, global (macroscopic) orientation of the nanotubes and polymers was not achieved as measured using X-ray diffraction experiments.[23] The poor orientation of PEO crystals along the fiber axis in the composite nanofibers was attributed to the poorly oriented nanotubes, which acted as nucleation agents for the PEO crystallization. A probabilistic modeling approach for the alignment of carbon nanotubes along the streamlines of the charged liquid jet was also proposed.[23] Achieving macroscopic orientation of MWNTs in the polymer matrix of nanofibers during electrospinning is a necessary step toward many meaningful technological applications. This is a major driving force for this research. Note that the concentric multiwalled carbon nanotubes used in the composite nanofiber sheets have typical outer diameters between 20 and 50 nm, while the procedures of the nanotube syntheses have been described in refs 24−26. Briefly, anthracene or toluene was pyrolyzed in the presence of a catalyst of ferrocene, $FeCl_3$, or $Fe(CO)_5$ during chemical vapor deposition.

This publication presents a new approach toward the production of highly aligned MWNTs embedded and well dispersed within electrospun PAN nanofibers. Direct assembly of composite nanofibers into large-area sheets is achieved by collecting the nanofibers onto a winder with a surface velocity larger than the velocity of electrospun nanofibers, which produces sheets of reasonably well-aligned nanofibers. Using combined techniques, we provide structural, morphological, and property evidence to illustrate the importance of the dispersion and orientation of a high concentration of MWNTs in the PAN nanofibers to produce composites with enhanced performance.

Results and Discussion

Morphology of MWNTs in Composite Nanofibers. Figure 1a shows a transmission electron microscope (TEM) bright field (BF) image of a composite nanofiber in which the surface-oxidized modified carbon MWNTs were embedded within the PAN nanofiber matrix. A 10 wt % concentration of MWNTs with respect to the PAN polymer [abbreviated as PAN/MWNT (90/10)] was electrospun into nanofibers. Since the MWNTs possess a high electron density compared with the PAN polymer matrix, the nanotubes appear as darker tubular structures embedded in the PAN nanofibers. A few MWNTs were observed with a diameter between 20 and 40 nm. They are aligned along the fiber axis of the nanofibers. The nanofibers had diameters of about 100−120 nm. The TEM BF image does not exhibit any interfacial delamination indicating that the interfacial bonding between the surface modified MWNTs and the PAN matrix was strong. The inset in Figure 1a is a selected-area electron diffraction (SAED) pattern obtained from the nanofiber in Figure 1a. The brightest inner diffraction spot pair is associated with the interlayer structure of the MWNTs at 0.336 nm. This is the (002) diffraction which is perpendicular to the fiber axis of the nanofiber in Figure 1a. The (004) diffraction was also identified outside of the (002) diffraction along the direction perpendicular to the fiber axis. It possesses half of the *d* spacing of the (002) diffraction. Along the fiber axis of the nanofiber, the (100) and the (110) diffractions were detected with *d* spacings of 0.213 and 0.123 nm, respectively. In addition, the (101) diffraction with a *d* spacing of 0.203 nm was observed on the quadrant. All diffraction spots are attributed to the characteristic diffraction patterns of the MWNTs. This shows that the surface-oxidation process did not destroy the crystalline structure of the MWNTs. The pair of the (002) diffractions is aligned perpendicular to the fiber axis of nanofiber, indicating that the long axis of MWNTs is aligned parallel to the fiber axis of the nanofiber as is also seen in electron micrographs.

(10) Chen, J.; Hamon, M. A.; Hu, H.; Chen, Y.; Rao, A. M.; Eklund, P. C.; Haddon, R. C. *Science* **1998**, *282*, 95.
(11) Saini, R. K.; Chiang, I. W.; Peng, H.; Smalley, R. E.; Billups, W. E.; Hauge, R. H.; Margrave, J. L. *J. Am. Chem. Soc*. **2003**, *125*, 3617.
(12) Kovtyukhova. N. I.; Mallouk, T. E.; Pan, L.; Dickey, E. C. *J. Am. Chem. Soc*. **2003**, *125*, 9761.
(13) Baskaran, D.; Mays, J. W.; Bratcher, M. S. *Angew. Chem., Int. Ed.* **2004**, *43*, 2138.
(14) Chen, R. J.; Zhang, Y.; Wang, D.; Dai, H. *J. Am. Chem. Soc*. **2001**, *123*, 3838.
(15) Star, A.; Stoddart, J. F.; Steuerman, D.; Diehl, M.; Boukai, A.; Wong, E. W.; Yang, X.; Chung, S.-W.; Choi, H.; Health, J. R. *Angew. Chem., Int. Ed.* **2001**, *40*, 1721.
(16) Durran, S.; Ajayan, P. M.; Blau, W.; Carroll, D. L.; Coleman, A. B.; Dalton, A. P.; Davey, A. P.; Drury, A.; McCarthy, B.; Maier, S.; Strevens, A. *Adv. Mater*. **1998**, *10*, 1091.
(17) Reneker, D. H.; Chun, I. *Nanotechnology* **1996**, *7*, 216.
(18) Bognitzki, M.; Czado, W.; Frese, T.; Schaper, A.; Hellwig, M.; Steinhart, M.; Greiner, A.; Wendroff, J. H. *Adv. Mater*. **2001**, *13*, 70.
(19) Schreuder-Gibson, H.; Senecal K.; Sennett, M.; Huang, Z.; Wen, J.; Li, W.; Wang, D.; Yang, S.; Tu, Y.; Ren, Z.; Sung, C. *Proc. Electrochem. Soc.* **2000**, 210.
(20) Seoul, C.; Kim, Y.-T.; Baek, C.-K. *J. Polym. Sci., Part B: Polym. Phys*. **2003**, *41*, 1572.
(21) Ko, F.; Khan, S.; Ali, A.; Gogotsi, Y.; Naguib, N.; Yang, G.; Li, C.; Shimoda H.; Zhou, O.; Bronikowski, M. J.; Smalley, R. E.; Willis, P. A. *AIAA* **2002**, 1426.
(22) Ko, F.; Gogotsi, Y.; Ali, A.; Naguib, N.; Ye, H.; Yang, G.; Li, C.; Willis, P. *Adv. Mater*. **2003**, *15*, 1161.
(23) Dror. Y.; Salalha, W.; Khalfin, R. L.; Cohen, Y.; Yarin, A. L.; Zussman, E. *Langmuir* **2003**, *9*, 7012.
(24) Hou, H.; Schaper, A. K.; Weller, F.; Greiner, A. *Chem. Mater*. **2002**, *14*, 3990.
(25) Hou, H.; Schaper, A. K.; Jun, Z.; Weller, F.; Greiner, A. *Chem. Mater*. **2003**, *15*, 580.
(26) Hou, H.; Zeng, J.; Weller, F.; Greiner, A. *Chem. Mater*. **2003**, *15*, 3170.

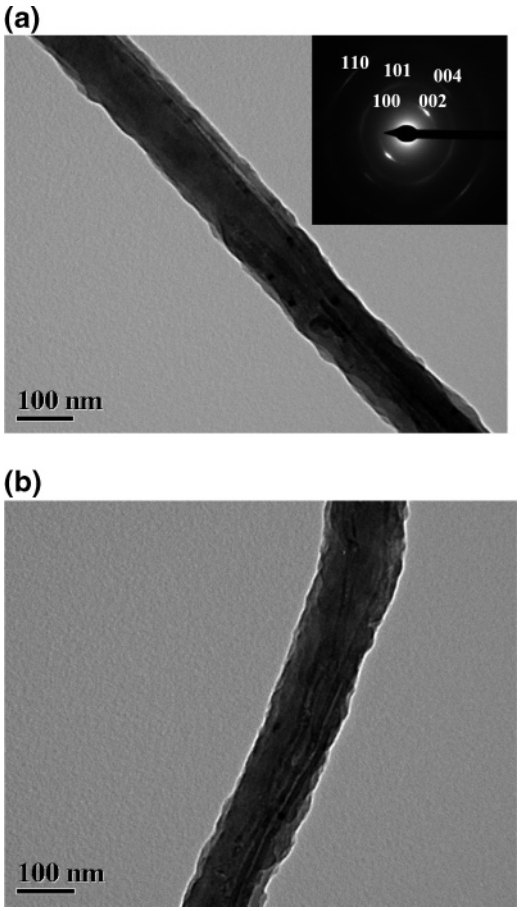

Figure 1. High magnification bright field TEM images of electrospun MWNT/PAN composite nanofibers containing (a) 10 wt % and (b) 20 wt % oxidized MWNTs (the scale bar of 100 nm). The inset in part a is an SAED pattern obtained from this nanofiber.

Figure 1b shows a composite nanofiber [PAN/MWNT (80/20)] which contains 20 wt % of surface-oxidized MWNTs. This MWNT concentration of the nanofibers is higher than those in previously reported studies.[19,23] In this figure, the diameters of MWNTs are between 20 and 30 nm, and they are oriented along the fiber axis of the nanofiber. The nanofiber has a diameter of approximately 100−120 nm. Since they are connected to each other by the PAN in the composite nanofibers, some MWNTs are bent or end-to-end to form an extended physical network. As compared with the pure PAN nanofibers (with diameters of 70−110 nm) obtained via electrospinning shown in the TEM BF image of Figure 2a, the composite nanofibers exhibited in Figure 1a and b have relatively rough surfaces. The smooth surface morphology of the pure PAN nanofiber was also observed in both the AFM height and phase images using tapping mode (see Figure 2b). The conductive MWNTs, containing a mixture of both the metallic and the semiconducting forms,[2] may further induce the formation of the rough surfaces of the composite nanofibers. The rough surface morphology observed on the composite nanofibers in TEM is consistent with a previous report of a rough, cobble-stone-like surface morphology for the PAN/SWNT nanofibers.[21] However, this surface morphology is quite different from that of polylactic acid (PLA)/SWNT composite nanofibers observed in TEM.[22] In these cases, the nanofibers are always "completely encapsulated" by the polymer. Where mechanical packing problems make a nanotube stick out, the "encapsulation" layer is very thin.

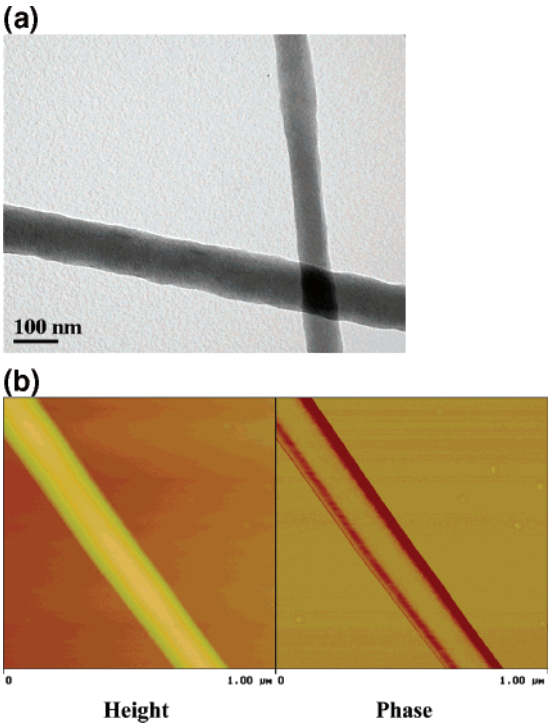

Figure 2. (a) High magnification BF TEM image and (b) the height and phase images from tapping mode AFM of electrospun pure PAN nanofibers.

In the AFM study, Figure 3a and c are the height image and profile of the surface morphology of a PAN/MWNT (90/10) fiber. Nonuniform streaked surface irregularities along the fiber axis of the nanofiber were observed in Figure 3a. The irregularities appear to be associated with the arrangement of the nanotube ends and with changes in the diameter of the nanofibers. Different thicknesses on the surface along the transverse directions can also be identified. In some places, the nanotubes may "poke through" the polymer surface. In these locations, the defects are evident. A height profile of the composite nanofiber along the cross section of the nanofiber of Figure 3a is shown in Figure 3c. This profile shows a more or less round shaped nanofiber with a diameter of ∼110 nm, while a skin surface roughness is a few nanometers in height and protruding defects (irregularities) are on a size scale of ∼10 nm. No clear multifaceted ribbon structures are observed in this figure.

In Figure 3b, the phase image exhibits several dark parallel streaks running along the fiber axis of the nanofiber with the different thicknesses along the perimeter of the nanofiber. Note that the phase difference along the transverse direction should be associated with the internal arrangement of the MWNTs within the PAN matrix and the nanotube ends "poking through" the polymer nanofibers. The dark parallel streaks in the AFM phase image may be due to the fact that the MWNTs are aligned near the skin layer of the nanofibers. The size of these streaks is more or less regular ranging between 20 and 30 nm, and this is comparable to the 20 to 40 nm diameter of the MWNTs. When the MWNTs are located near the skin layer of the composite nanofiber, the tapping mode of AFM is able to "feel" the embedded MWNTs due to different mechanical moduli of the MWNTs and the PAN matrix and therefore generate the recognizable dark streak features in Figure 3b. The surface defects across the transverse direction of the nanofiber observed in the phase image of Figure 3b could be associated with the

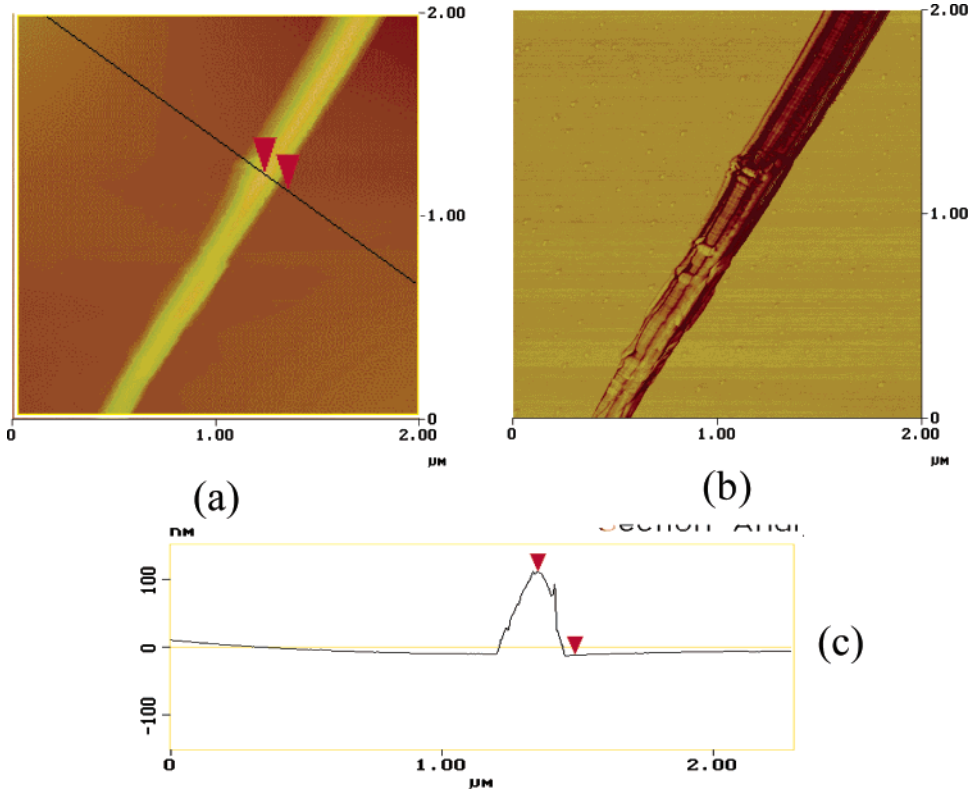

Figure 3. Tapping mode AFM images of a PAN/MWNT composite nanofiber containing 10 wt % modified nanotubes: (a) a height image, along with a line showing the position for the nanofiber cross-section profile analysis, (b) the corresponding phase image, and (c) a height profile cross the nanofiber of part a.

concentration of the MWNTs, the DMF evaporation rate, and the resulting packing of the MWNTs in the PAN matrix during electrospinning.

Interfacial Bonding, Structure, and Orientation of MWNTs in Nanofibers. In Figure 4, plots a−c show the UV/vis absorption spectra of a pure PAN nanofiber sample dissolved in DMF, surface-oxidized MWNTs dispersed in DMF, and a mixture of the PAN and surface-oxidized MWNTs in DMF, respectively. In Figure 4 plot a, the absorption band at 274 nm for the PAN/DMF solution is attributed to the C≡N π-absorption. The major absorption bands of the dispersed MWNTs in DMF as seen in plot b are at 283 and 1020 nm. Minor shoulder absorptions also occur at ∼360−370 nm. These absorptions originate from the surface-oxidized MWNTs and are attributed to a π-plasmon band and a semiconducting nanotube transition band gap.[27−30] However, the mixture of the PAN and surface-oxidized MWNTs in DMF exhibits extensive fine absorption structures as shown in plot c. The absorption bands are observed at 280 nm, 315 nm, 387 nm, 424 nm, 577 nm, and ∼960 nm. The absorption band at 280 nm is close to that observed in the surface-oxidized MWNTs dispersed in DMF in plot b. Furthermore, the broad absorption at 1020 nm in the UV/vis absorption is evidence that the MWNTs are laterally packed into small bundles.[27] On the other hand, the broad band at 960 nm in the

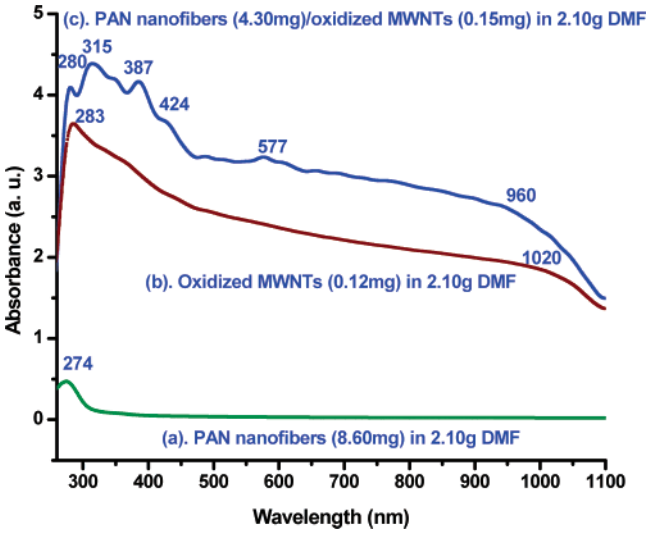

Figure 4. UV/vis spectra recorded at room temperature of the following: (a) a PAN solution in DMF (0.41 wt %), (b) a mixture of 0.0057 wt % MWNTs in DMF after sonication, and (c) a mixture of 0.0071 wt % MWNTs and 0.20 wt % PAN in DMF.

mixture of the PAN with surface-oxidized nanotubes (plot c) is a blue-shift of the 1020 nm band observed for the MWNT/DMF solution in plot b. This shift indicates that the nanotube bundles have been separated from each other and stabilized, via PAN molecular wrapping. This could be similar to that seen in SDS-wrapped SWNTs in SWNT/SDS micelle systems.[27] The extensive fine absorption bands observed in UV/vis, therefore, suggest the formation of charge-transfer complexes between the surface-oxidized MWNTs and the PAN molecules through the delocalization of π-electrons along the conjugated sequences.

(27) O'Connell, M. J.; Bachillo, S. M.; Huffman, C. B.; Moore, V. C.; Strano, M. S.; Haroz, E. H.; Rialon, K. L.; Boul, P. J.; Noon, W. H.; Kittrell, C.; Ma, J.; Hauge, R. H.; Weisman, R. B.; Smalley, R. E. *Science* **2002**, *297*, 593.
(28) Strano, M. S.; Dyke, C. A.; Usrey, M. L.; Barone, P. W.; Allen, M. J.; Shan, H.; Kittrell, C.; Hauge, R. H.; Tour, J. M.; Smalley, R. E. *Science* **2003**, *301*, 1519.
(29) Pichler, T.; Knupfer, M.; Golden, M. S.; Fink, J.; Rinzler, A.; Smalley, R. E. *Phys. Rev. Lett.* **1998**, *80*, 4729.
(30) Ajayan, P. M.; Iijima, S.; Ichihashi, T. *Phys. Rev. B* **1993**, *47*, 6859.

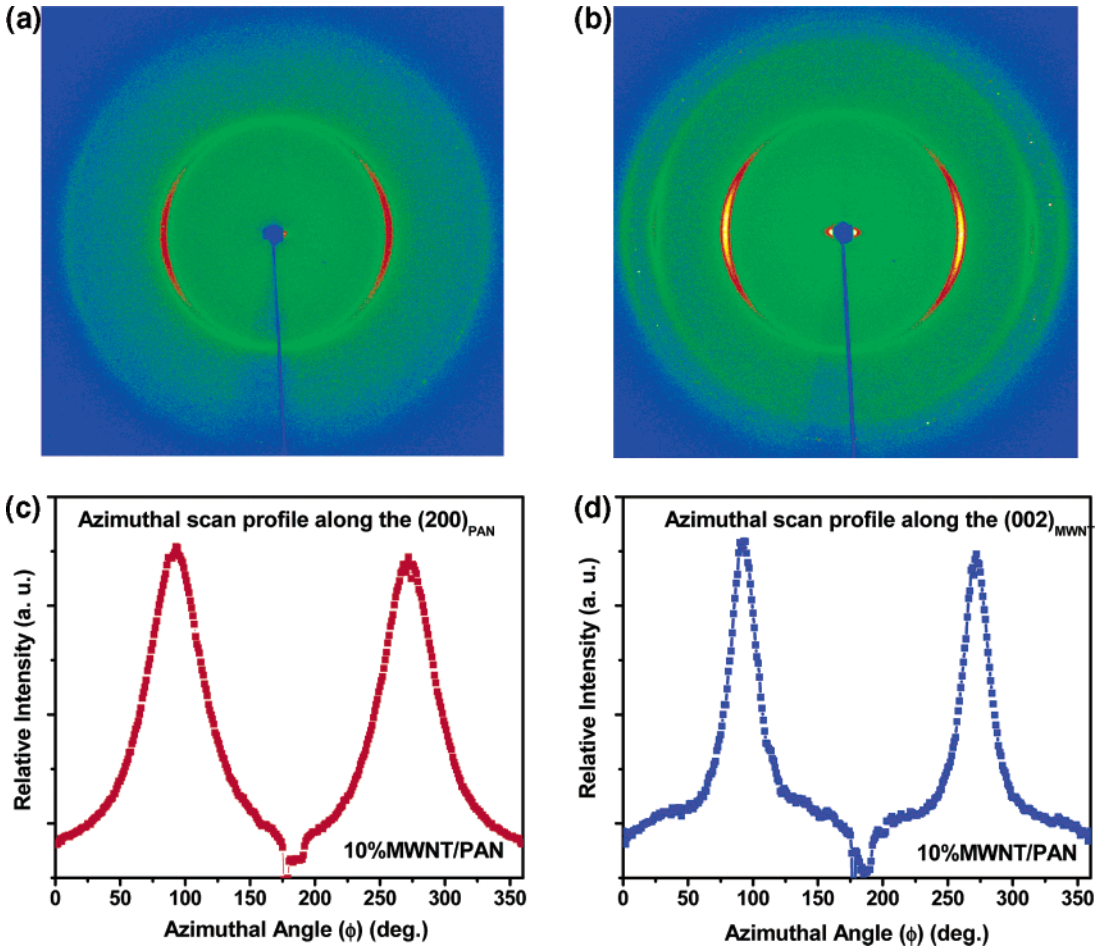

Figure 5. Two-dimensional WAXD patterns of electrospun composite nanofiber sheets containing the following: (a) PAN, (b) 10 wt % MWNTs in PAN, (c) the azimuthal scan of the $(200)_{PAN}$ diffraction ring from part b, and (d) the azimuthal scan of the $(002)_{MWNT}$ diffraction ring from part b.

This is similar to the formation of charge-transfer complexes, observed: in conjugated conducting polyisoprene and iodine doping agents;[31] in the $SWNT^{+}/OsO_4^{-}$ with the preferential functionalization of metallic nanotubes;[32] or in amylose-SWNT complexes with the evidence of the blue color change in the 200−800 nm range.[33] When the negatively charged −C≡N: groups in PAN are attached onto the MWNTs, charge-transfer complexes form between the MWNTs and the attached PAN molecules. Note that the anion−π-electron interactions have also been reported.[34] Although we have not completely ruled out the interactions between the *p*-doped nanotubes with the residual $FeCl_3$ catalyst (used as a catalyst for growing carbon nanotubes) and the polymers, we have not detected this type of interaction in our control experiments.

The 2D WAXD patterns obtained from the electrospun PAN/MWNT composite sheets are shown in Figure 5. Note that the X-ray beam is directed parallel to the sheet normal and, thus, the beam is also perpendicular to the winding direction of the sheet. The composite nanofibers in the sheet were highly oriented along the winding direction of the rotating drum collector. Figure 5a shows a 2D WAXD pattern for nanofiber sheets electrospun from pure PAN. A pair of intense arcs is observed at $2\theta = 17.18°$, while a pair of relatively weak arcs is seen at $2\theta = 29.98°$, but both of them are on the equator. They correspond to *d* spacings of 0.516 nm and 0.298 nm, respectively. These two pairs of diffractions can be assigned as the (200) and the (020) planes of the ordered structure of PAN. Therefore, a 2D rectangular lattice with $a = 1.03$ nm and $b = 0.60$ nm can be deduced. These dimensions can be compared to those determined via PAN single crystals of $a = 1.06$ nm and $b = 0.58$ nm based on the SAED results reported.[35] The dimensions of the PAN ordered structure in the nanofibers are 2.6% smaller along the *a*-axis and 2.8% larger along the *b*-axis, as compared to those of the PAN single crystals.

For the PAN/MWNT (90/10) composite nanofiber sheets, Figure 5b shows a pair of additional intense diffraction arcs on the equator at $2\theta = 26.50°$. The *d* spacing is calculated to be 0.336 nm. This is identified as the (002) diffraction of the MWNTs. The layer normal of carbon graphite sheets in the nanotubes is perpendicular to the fiber axis of the nanofibers, as observed in the SAED pattern of Figure 1a. A quantitative orientation factor (*f*) can thus be calculated based on Herman's orientation equation $f = (3\langle\cos^2\varphi\rangle - 1)/2$, where the average angle between the molecular axis and the fiber direction is defined as $\langle\varphi\rangle$.[36] This requires azimuthal scans of individual

(31) Dai, L. *J. Phys. Chem.* **1992**, *96*, 6469.
(32) Banerjee, S.; Wong, S. S. *J. Am. Chem. Soc.* **2004**, *126*, 2073.
(33) Star, A.; Steuerman, D.; Health, J. R.; Stoddart, J. F. *Angew. Chem., Int. Ed.* **2002**, *41*, 2508.
(34) QuiEonero, D.; Garau, C.; Rotger, C.; Frontera, A.; Ballester, P.; Costta, A.; Dey, P. M. *Angew. Chem., Int. Ed.* **2002**, *41*, 3389.
(35) Geil, P. H. *Polymer Single Crystals*; John Wiley & Sons: New York, 1973.
(36) Samuels, R. J. *Structured Polymer Properties: the Identification, Interpretation, and Application of Crystalline Polymer Structure*; John Wiley & Sons: New York, 1974.

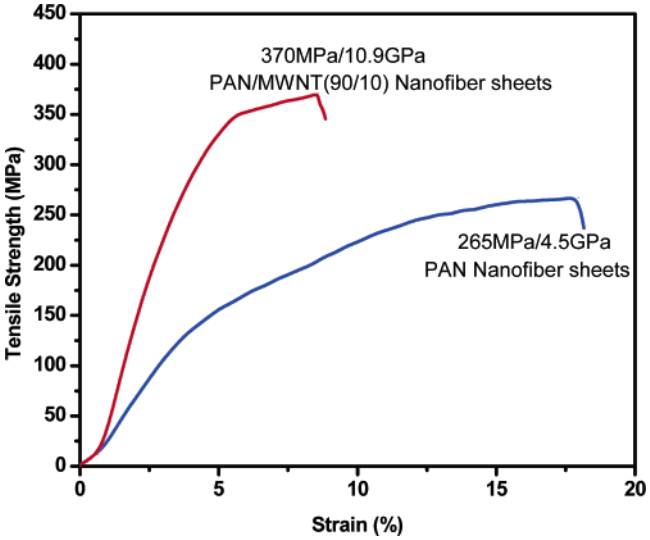

Figure 6. Stress−strain curves at ambient temperature for compressed pure PAN and for PAN/MWNT(90/10) composite nanofiber sheets.

diffraction arcs for both the $(200)_{PAN}$ and the $(002)_{MWNT}$ in Figure 5b, and they are shown in Figure 5c and d, respectively. The full width at half-maximum (fwhm $= \omega$) of the PAN in composite nanofiber sheets is $\omega = 52°$ (in Figure 5c). The fwhm for the MWNTs is $\omega = 25°$ (in Figure 5d). These correspond to an orientation factor for the surface-oxidized MWNTs of $f_{MWNT} = 0.90$ and an orientation factor for the PAN crystal structure of $f_{PAN} = 0.62$, respectively. The orientation of MWNTs in the nanofibers is thus significantly higher than that of the PAN crystal structure. This suggests that the nanotubes are aligned in the confined nanofibers during electrospinning, and therefore, they are parallel to the fiber axis of the nanofibers, while the PAN is aligned by crystallization onto nuclei oriented by the flow and elongation of the electrospinning process.[23] Note that the nucleation sites may relax as well as the MWNTs during the solidification process of the nanofibers, while the surface tension of the fluid jet tends to align the MWNTs with the axis of the fluid jet as the diameter of the jet decreases. During the electrospinning, the orientation of the small PAN crystals can therefore relax faster than the orientation of the MWNTs, and as a result, the MWNTs retain a higher orientation in the nanofibers compared with the PAN crystals.

To the best of our knowledge, this is the highest degree of orientation for nanotubes in electrospun composite nanofibers achieved in composite sheets on a macroscopic scale. This degree of orientation in the electrospun PAN/MWNTs nanofiber sheets approaches that observed in the PAN/SWNT microfibers made by a dry-jet spinning method when the draw ratio reaches 4.3 times.[8]

Enhanced Macroscopic Properties in Composite Nanofiber Sheets. Figure 6 shows two representative plots of stress versus strain for the pure PAN and the PAN/MWNT (90/10) nanofiber sheets compressed at 100 °C. The pure PAN nanofiber sheets exhibit a tensile strength of 265 MPa. The strain at break is 17.8%, and the tensile modulus is 4.5 GPa. As the concentration of the surface-oxidized MWNTs increases, the tensile modulus and strength increase while the strain at break decreases. The detailed mechanical property data are listed in Table 1, in which each data point was obtained by averaging the results of five test samples. When the MWNT concentration

Table 1. Tensile Strength, Tensile Modulus, and Elongation of Compressed Neat PAN and Composite PAN/MWNT Nanofiber Sheets

PAN/MWNT	diameter (nm)	tensile strength (GPa)	tensile modulus (GPa)	elongation at break (%)
100/0	50−300	265	4.5	17.8
97/3	50−300	312	6.4	12.8
95/5	50−300	366	9.8	9.9
90/10	50−300	370	10.9	8.2
80/20	50−300	285	14.5	4.4

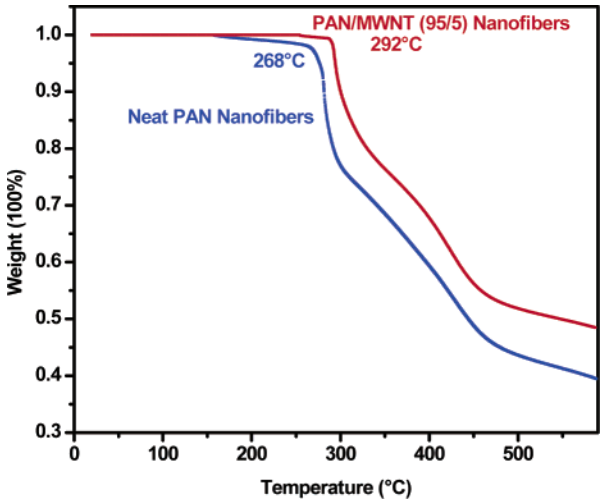

Figure 7. Thermogravimetric analysis (TGA) curves for pure PAN and for PAN/MWNT (95/5) composite nanofiber sheets in a N_2 atmosphere at a heating rate of 10 °C/min.

is increased to 10 wt %, the compressed sheet samples exhibit a significant modulus improvement of up to 10.9 GPa, while the tensile strength increases to 370 MPa and the strain at break decreases to 8.2%. The highest tensile modulus achieved was 14.5 GPa for the PAN/MWNT (80/20) samples, while the tensile strength remained at 285 MPa and the strain at break was about 4.4%. The tensile moduli for PAN/MWNT (90/10) and PAN/MWNT (80/20) samples are about 3 to 4 times higher than that of the pure PAN nanofiber sheets. Note that the highest tensile modulus reported for the SWNT bundle based microfiber ribbons[5] is ∼15 GPa and that for the PAN/SWNT (90/10) macrofibers is ∼16 GPa.[8] Our nanofiber mechanical properties are close to the reported value. It is interesting to know whether the mechanical properties can be further enhanced with the improved interfacial bonding, orientation, and uniformity, and this will be our future work.

Since the MWNTs are conductive, the PAN/MWNT (90/10) and (80/20) sheets possess electrical conductivities of up to 0.1 and 0.5−1.0 S/cm, respectively, at ambient temperature. The conductivity values are about 2 orders of magnitude higher than those of corresponding isotropic PVA/MWNT composite films.[37] Note that the electrical conductivity for the PAN/MWNT (80/20) composite nanofiber sheets is only about 1 order of magnitude lower than that for the SWNT bundle-based microscopic fiber ribbons (about 10 S/cm).[5] Since electrical conductivity requires a percolating network be formed by the MWNTs, it is concluded that the composite nanofibers, at a concentration of 10 wt % MWNTs, start to form the percolating network.

(37) Shaffer, S. P.; Windle, A. W. *Adv. Mater.* **1999**, *11*, 937.

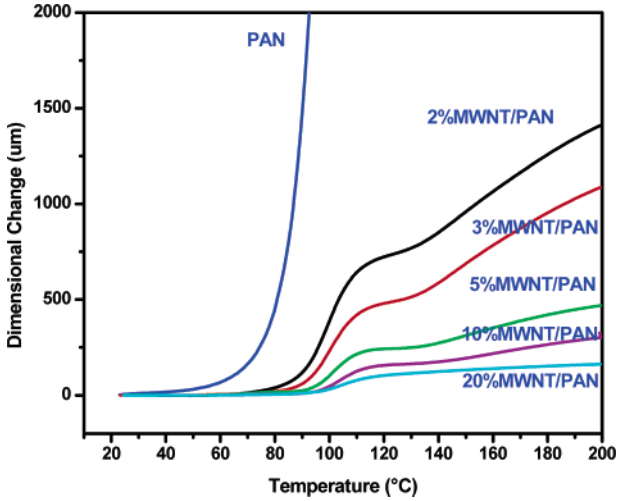

Figure 8. Thermal mechanical analysis (TMA) results of surface-oxidized MWNT/PAN composite nanofiber sheets containing MWNTs of 0, 2, 3, 5, 10, and 20 wt %, aligned along the nanofiber winding direction.

These conductive PAN/MWNT sheets have potential applications in conductive nanoelectrodes, supercapacitors, and nanosensors.[2]

The thermogravimetric behavior of the PAN/MWNT sheets was investigated. The dispersion of surface-oxidized MWNTs into the PAN matrix leads to an increase in thermal stability measured, in a N_2 atmosphere at a heating rate of 10 °C/min, as shown in Figure 7. The onset temperature for decomposition shifts from 268 °C for the pure PAN nanofibers to 292 °C for the PAN/MWNT (95/5) nanofibers in a N_2 atmosphere. This suggests that the nanofiber structural changes take place due to the presence of the carbon nanotubes,[21,22] which seems to be consistent with the formation of charge-transfer complexes in our experimental observations. However, the driving force behind the possible structural change has yet to be determined.[8,21,22]

The thermal mechanical performance of the PAN/MWNT composite nanofiber sheets containing 0, 2, 3, 5, 10, and 20 wt % surface-oxidized nanotubes was measured in TMA under an external tension of approximately 4 GPa as shown in Figure 8. The thermal deformation or softening temperature was determined to be 83 °C in the pure PAN nanofiber sheets which is close to a T_g of 85 °C reported for bulk PAN materials. Above the T_g, a liquidlike (flow) deformation was detected in TMA with a large dimensional change as shown in Figure 8. As the concentration of the MWNTs increases, the deformation above the T_g is suppressed and the thermal dimensional stability of the composite nanofiber sheets at high temperature increases.

In addition, the thermal deformation temperature (that is close to the T_g in the pure PAN) shifted from 83 °C to 94 °C when the concentration of the oxidized nanotubes was increased to 10 wt % in the composite nanofiber sheets, as shown in Figure 9a. The reason for the increase in T_g of the composite nanofiber sheets suggests that restricted molecular segmental motions occur at the interface between the nanotubes and the PAN due to the formation of the charge-transfer complexes. When the segmental motions of the PAN long chains are restricted by the surface-oxidized nanotubes through physical and/or chemical interactions, the T_g is expected to increase. The thermal expansion coefficient (CTE) of the PAN/MWNT composite nanofiber sheets also decreases from 180×10^{-6}/°C in the pure PAN nanofiber sheets to 27, 17, and 13×10^{-6}/°C along the winding direction, as shown in Figure 9b, when the MWNT loading is increased to 5, 10, and 20 wt %, respectively. More interestingly, along the nanofiber winding direction, the 1D axial CTE values of PAN/MWNT composite nanofibers are on the same order of magnitude of Al (27.0×10^{-6}/°C), Cu (17.0×10^{-6}/°C), and Ti (12.5×10^{-6}/°C) in the solid state.

Conclusions

In summary, this work describes the fabrication of continuous composite nanofiber sheets containing surface-oxidized nanotubes without using any surfactants or binding agents. Such PAN/MWNT composite nanofiber sheets represent an important step toward utilizing carbon nanotubes in materials to achieve remarkably enhanced physical properties. A high degree of orientation for the MWNTs in the PAN/MWNT nanofibers is identified via both TEM and 2D WAXD data. The degree of orientation for the surface-oxidized MWNTs in the nanofibers is significantly greater than that of the PAN matrix crystals in

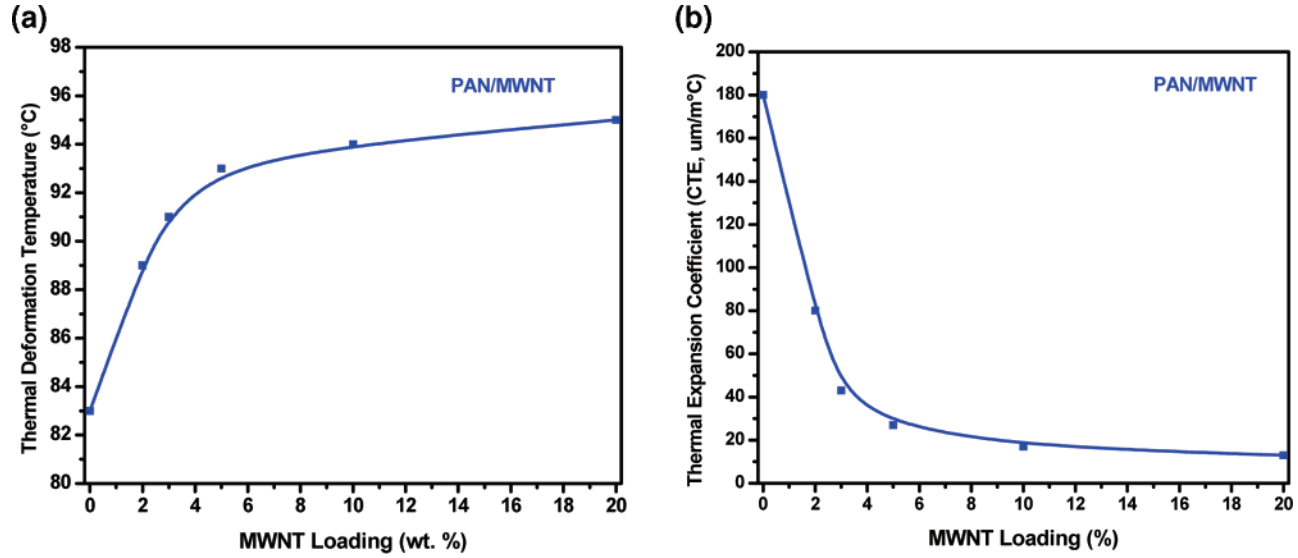

Figure 9. Thermal deformation temperature (a) and thermal expansion coefficient (CTE) (b) of surface-oxidized MWNT/PAN composite nanofiber sheets as a function of the oxidized MWNT content, along the axis of the aligned nanofibers.

the nanofibers ($f_{MWNT} = 0.90$ for the MWNTs versus $f_{PAN} = 0.62$ for the ordered structure of PAN). This can be explained by the structural formation during the electrospinning processes and different relaxation of orientation behaviors of the MWNTs and PAN crystals. The extensive fine absorption structure observed in UV/vis experiments reveals the formation of charge-transfer complexes at the interfaces between the surface-oxidized MWNTs and the surrounding PAN molecules. Incorporation of the MWNTs into the nanofibers increases the electrical conductivity to ~1.0 S/cm for PAN/MWNT (80/20) sheets. Thermal stability also increases. The onset temperature for the decomposition is at 268 °C for the pure PAN nanofibers and at 292 °C for the PAN/MWNT (95/5) nanofibers in a N_2 atmosphere. The thermal expansion coefficient decreases from 180×10^{-6}/°C in the pure PAN nanofiber sheets to 17×10^{-6}/°C and 13×10^{-6}/°C for the PAN/MWNT (90/10) and (80/20), respectively. The tensile modulus is 14.5 GPa for PAN/MWNT (80/20) sheets. These enhanced macroscopic properties characterize new high performance nanotechnology based composite materials.

Acknowledgment. This work was supported by the Collaborative Center in Polymer Photonics between Air Force Research Laboratory Materials and Manufacturing Directorate and The University of Akron. S.Z.D.C. acknowledges the support of NSF (DMR-0203994). Preparation of the nanotubes was supported by NSF DMII-MPM 0100354 and by DOE Rex Ramsier's Project. J.J.G. thanks Dr. Liming Dai for his helpful discussions on the interfacial structure formed between the surface-oxidized nanotubes and PAN.

Supporting Information Available: Additional information on the entire Experimental Section. This material is available free of charge via the Internet at http://pubs.acs.org.

JA048648P